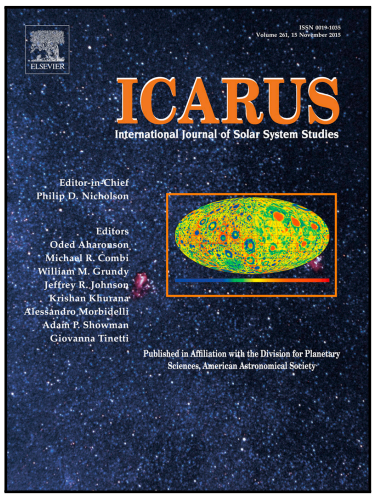

UV luminescence characterisation of organics in Mars-analogue substrates

B. Laurent , C.R. Cousins , M. Gunn , C. Huntly , R. Cross , E. Allender

PII: S0019-1035(18)30470-6
DOI: https://doi.org/10.1016/j.icarus.2018.12.031
Reference: YICAR 13147

To appear in: *Icarus*

Received date: 11 July 2018
Revised date: 7 December 2018
Accepted date: 12 December 2018

Please cite this article as: B. Laurent , C.R. Cousins , M. Gunn , C. Huntly , R. Cross , E. Allender , UV luminescence characterisation of organics in Mars-analogue substrates, *Icarus* (2018), doi: https://doi.org/10.1016/j.icarus.2018.12.031

Highlights

- UV photo luminescence detection of PAHs is possible within synthetic and natural gypsum, and synthetic halite.

- The most transparent minerals are more conducive to UV photoluminescence detection of trapped organic matter.

- Iron oxide hampers but does not completely quench the UV photoluminescence emission.

- The maturity of organic carbonaceous material influences the luminescence response, resulting in a reduced signal for UV excitation wavelengths down from 375 nm to 225 nm.

•

UV luminescence characterisation of organics in Mars-analogue substrates

B. Laurent[1,2], C.R. Cousins[1] , M. Gunn[2]., C. Huntly[2], R. Cross[2]., E. Allender[1,2].

[1]School of Earth and Environmental Sciences, North Street, University of St Andrews, St Andrews, Fife, UK, KY16 9AL.

[2] Institute for Mathematics and Physics, Aberystwyth University, Aberystwyth

Running title: UV luminescence of Mars analogues

Corresponding author: Dr Boris Laurent; Email: bcdl@st-andrews.ac.uk

Abstract

Detection of organic matter is one of the core objectives of future Mars exploration. The ability to probe rocks, soils, and other geological substrates for organic targets is a high priority for *in situ* investigation, sample caching, and sample return. UV luminescence – the emission of visible light following UV irradiation – is a tool that is beginning to be harnessed for planetary exploration. We conducted UV photoluminescence analyses of (i) Mars analogue sediments doped with polyaromatic hydrocarbons (PAHs; <15 ppm), (ii) carbonaceous CM chondrites and terrestrial kerogen (Type IV), and (iii) synthetic salt crystals doped with PAHs (2 ppm). We show that that detection of PAHs is possible within synthetic and natural gypsum, and synthetic halite. These

substrates show the most apparent spectral modifications, suggesting that the most transparent minerals are more conducive to UV photoluminescence detection of trapped organic matter. Iron oxide, ubiquitously present on Mars surface, hampers but does not completely quench the UV luminescence emission. Finally, the maturity of organic carbonaceous material influences the luminescence response, resulting in a reduced signal for UV excitation wavelengths down to 225 nm. This study demonstrates the utility of UV luminescence spectroscopy for the analysis of mixed organic-inorganic materials applicable to Mars exploration.

Keywords: UV luminescence; Mars; Analogue; Spectroscopy; Organic

1. Introduction

The detetction of organic compounds within near-surface crustal materials on Mars is a key aim for current (e.g. NASA Mars Science Laboratory) and future (e.g. NASA Mars2020 and ESA ExoMars 2020) missions. Delivery of exogenic organic matter is a daily process on Mars (up to $4x10^{-4}$ g. $m^{-2}yr^{-1}$; Flynn and McKay, 1990), delivered by comets, asteroids and IDPs ($0.013.10^6$, $0.05.10^6$ and $0.07 - 0.3.10^6$ kg/yr respectively; Frantseva et al. 2018). Furthermore, endogeneous macromolecular reduced carbon has been identified in the Tissent SNC meteorite (Steele et al. 2012). One of the remaining obstacles in assessing Martian habitability is the relative difficulty in detecting organic carbon compounds at the Martian surface. This difficulty remained until the recent detection of thiophenic, aromatic, and aliphatic complex compounds at Gale Crater (Eigenbrode et al. 2018),

adding to previous detections of trace atmospheric methane (Webster et al. 2015; 2018), chlorobenzene (Freissinet et al. 2015; Millan et al. 2016), and chlorinated hydrocarbons (Glavin et al. 2013). Such *in situ* detection however still faces two main challenges; (i) the oxidizing nature of the Martian soil coupled with on-board pyrolysis techniques employed for analysis (e.g. Sample Analysis at Mars; Mahaffy et al. 2012), and (ii) degradation of organic compounds by ionizing irradiation (Dartnell et al. 2007, Ten Kate 2010). This dual challenge is being mitigated, in part, through the development of new spectroscopic techniques (e.g. Storrie-Lombardi et al. 2009, Eshelman et al. 2017; Uckert et al. 2018), coupled with physical access to the martian subsurface, such as the 2 m drill on board the ExoMars 2020 rover (Vago et al., 2017).

Distinct UV-excited photoluminescence spectra are emitted by many organic molecules, ranging from polyaromatic hydrocarbons (PAHs), to some amino-acids, as well as more complex mixtures of dissolved organic matter (DOM) (Chen et al. 2003, Rivera-Figueroa et al. 2004, Carrier et al. 2016, Eshelman et al. 2014, 2015, 2017). In addition, inorganic substrates can also produce a photoluminescence response following UV excitation (Gaft et al. 2015). UV photoluminescence (UV PL) therefore has the potential to become a powerful tool in the search for organic molecules, and potentially biosignatures, at the Martian surface (Storrie-Lombardi et al. 2010; Dartnell et al. 2011, 2012; Sephton and Carter 2015). UV PL results from the complete absorption of a photon generating an electron hole pair followed by recombination and radiative emission at a longer wavelength.The ultraviolet photoabsorbtion cross section is much higher than the Raman scattering cross section, where generally one scattered photon out of 10^7 has a Raman shift (Ball, 2002). Consequently, UV PL can provide information at detection thresholds as low as ppt concentrations for PAHs using laser induced luminescence (Richardson and Ando, 1977). As such, UV luminescence spectroscopy is becoming an increasingly popular technique for *in-situ* Mars exploration. The Optical Microscope on the NASA Phoenix lander (operational in 2008) used near-UV (NUV; λ_{ex} = 360–390 nm) LED

illumination to investigate samples of the Martian regolith, but failed to find any mineral or organic luminescent material (Goetz et al. 2012). This unsuccessful detection was potentially due to the Fe-rich nature of the Martian regolith (Fe^{2+} and Fe^{3+} can both suppress luminescence, Gaft et al. 2015). Alternatively, the relatively long excitation wavelengths used, and the likely absence of organic material immediately at the Martian surface could have hindered detection. Since then, UV PL imaging capability (λ_{ex} = 365 nm) has been incorporated into the Mars Hand Lens Imager (MAHLI) on NASA's MSL Curiosity rover (Edgett et al. 2012). MAHLI has been used to demonstrate the relevance of NUV excitation sources, and especially 365 nm excitation for the detection of fluorescent minerals in thin sections of Martian meteorites (Minitti and McCoy 2012) and at Gale Crater (Fisk et al. 2015). Regarding upcoming exploration, future instruments are in development, including the Scanning Habitable Environments with Raman & Luminescence for Organics & Chemicals ("SHERLOC") instrument, which will be part of the payload for the NASA Mars 2020 Rover mission (Beegle et al., 2015). This instrument is a deep UV (λ_{ex} =248.6 nm) Raman and Luminescence imaging spectrometer (Beegle et al., 2015), and will be the first dedicated spectrometer with UV capability to be deployed at the martian surface. UV PL spectroscopy and imaging capabilities have also been previously considered for the European Space Agency ExoMars Panoramic Camera (Storrie-Lombardi et al., 2009), and hyperspectral imaging instrument concepts (Barnes et al., 2014). The applicability and limitations of UV PL for the analysis of planetary analogue materials however are relatively unknown in comparison to other spectroscopic techniques, such as Raman and Visible to Near Infrared (VNIR) reflectance spectroscopy. UV-Raman can be used to detect potential biomarkers (e.g. pigments, amino acids) when mixed with Martian analogue minerals (for organic concentrations > 10 wt. %, Skulinova et al. 2014). UV-Raman has also been shown to detect aromatic hydrocarbons, embedded in Martian analogue soil at a concentration of 0.1 wt. % (Abbey et al, 2017). UV PL is complementary to such techniques, as the higher luminescence response enables lower detection limits, but typically with less information conveyed than the weaker Raman scattering signal. PAHs in particular have been the focus of recent studies, primarily due to their widespread presence in the interstellar

medium (Ehrenfreund et al., 2011) and carbonaceous chondrites (Becker et al, 1997), and possession of a strong luminescence response following UV excitation (Muller et al, 2011; Dartnell et al. 2012).

Mars surface mineralogy is characterized by largely basaltic igneous lithologies and hydrated mineral phases, namely phyllosilicates and sulfates, which together characterise all recent and future landing sites (Arvidson et al, 2006; Ehlmann *et al.* 2008; Ehlmann et al, 2012; Golombek and McSween 2014). In addition, a global iron-oxide rich regolith is ubiquitous (Bell et al, 2000), while hematite concretions have been identified in multiple localities (Meridiani Planum, Klingelhöfer et al. 2004). To this end, Mars surface processes over time have been broadly divided into three mineralogical 'epochs' that reflect global environmental change: the phyllosian, theiikian, and siderikian (Bibring et al., 2006), with clay-bearing lithologies identified as the most likely substrates for preservation of ancient organic material (Ehlmann et al., 2008). One of the most widespread sulfates found on Mars is calcium sulfate, in locations such as Olympia Planitia, Mawrth Vallis, Columbus crater and Gale crater (Langevin et al, 2005, Loizeau et al, 2007; Wray et al, 2011; Nachon et al, 2014; Rapin et al., 2016). Likewise, magnesium sulfates such as epsomite ($MgSO4{\cdot}7H2O$), and sodium chloride (NaCl) salts are present on Mars (Vaniman et al. 2004, Gandrin et al. 2005, Osterloo et al. 2010). Little is known about the luminescence response of organic molecules hosted within such sedimentary and crystalline substrates. Furthermore, iron oxide has been shown to act as a UV luminescence quencher (Gaft et al. 2015), potentially affecting the overall ability of UV PL techniques to detect organics hosted within or among Fe^{3+} bearing minerals. We investigated the UV luminescence spectra of Mars-analogue materials both with, and without, the addition of PAHs anthracene, perylene, and pyrene, as well as carbonaceous

chondrites and terrestrial type IV kerogen, which are representative of exogenously-delivered and geologically recalcitrant carbonaceous material, respectively.

2. Methods

2.1 Samples

2.1.1 Sedimentary substrates

Three Mars analogue sediments from Iceland were selected to broadly represent the three key mineralogical groups on Mars: phyllosilicates, sulfates, and iron oxides. The three analogues consist of (i) gypsum from a late-stage mineral vein at the Namafjall geothermal ridge (Harris et al., 2015), (ii) paleolacustrine clay-bearing mud-siltstone, and (iii) iron oxide soils from the Namafjall geothermal field (Harris et al., 2015). Samples were powdered (<500 µm grainsize) and homogenized in an alumina pestle and mortar, and half of the resulting powders doped with one of two PAHs: five-ringed perylene and three-ringed anthracene, (Sigma Aldrich; PAH solutions in methanol, with a concentration of 2000 and 200 µg/ml for perylene and anthracene respectively) to a final concentration of 15 ppm. Samples were homogenized again following PAH doping. Doped and reference blank samples were pressed into copper samples holders with wells 0.4 cm diameter x 0.25 cm depth for low-temperature UV PL analysis**.**

2.1.2 Synthetic salt crystals

Epsomite and halite crystals were precipitated from saturated (1.3 g/ml for $MgSO_4 \cdot 7H_2O$; 0.4 g/ml for NaCl) solutions at 40 °C. Once cooled to room temperature, the solutions were doped with either anthracene or pyrene (Sigma Aldrich; PAHs solutions in methanol, at 200 µg/mL and 100 µg/mL for anthracene and pyrene respectively), for a final PAH concentration of 2 ppm. To investigate the effect of Fe-oxyhydroxides on the UV PL response, duplicate PAH-doped salt samples were synthesized with the addition of the Fe-oxyhydroxide 'Oxide' sediment from the Namafjall geothermal field, described above. Saturated solutions were doped with between 0.15 – 0.2 g/ml Fe-oxyhydroxide and the magnesium sulfate solutions with 0.2 g/ml. The resulting crystal sizes averaged 2 x 1 mm for epsomite and 2 x 2 mm for halite.

2.1.3 Carbonaceous chondrites

Three CM2 carbonaceous chondrite chips were included in the study to investigate the UV PL properties of one of the exogenous sources of organic material delivered to the Martain surface. These were the Meteorite Hills MET01072 meteorite (0.49 g) and the Alan Hills meteorite ALH84044 (1.045 g), loaned from NASA JSC, USA, and Murchison (1 g) loaned from the Natural History Museum, UK. CM chondrites are primitive chondrites, formed from low temperature (<100 °C, Guo and Eiler, 2007) and have experienced aqueous alteration after accretion on the parent-body. The least altered sample is Murchison, with the highest aqueous alteration index (2.5) compared to MET01072 and ALH84044 (respectively 2.3 and 2). Using the degree of hydration (Water/OH) detailed in Alexander et al. (2013), Murchison has a ratio of 0.96, ALH84044 a ratio of 1.24 and MET01072 a ratio of 1.04. CM MET01072 has also undergone impact deformation (Lindgren et al. 2015). The total organic carbon concentration of MET01072 and ALH84044 are comparable (1.7 %, Alexander et al. 2013),

and higher in the case of Murchison (2.1 %). The two finds, MET01072 and ALH84044 exhibit respectively a moderate (B) and limited (Ae) weathering, and Fayalite content is between 0-1 mol. % for Murchison (Fuchs et al, 1973), 0-12 mol. % for MET01072 and 0-2 mol. % for ALH84044 (NASA Astromaterials Research and Exploration Science database). Murchison is one of the most studied carbonaceous chondrites, with a mineralogy of porphyritic millimetre-size chondrules dominated by ferromagnesian silicates, and fine-grained phyllosilicate rich matrix, where carbonates and iron-nickel grains are present (Lindgren et al. 2015). The organic content of Murchison is dominated by the insoluble fraction (IOM), consisting of small aromatic units (2 or 3 on average) linked by short aliphatic moieties (Derenne and Robert, 2010). The organic carbon is close to being purely graphitic (> 99 %, Pizzarello and Shock, 2010). The soluble fraction is composed of amino acids or polyols, hydrocarbons and extends over thousands of different molecular compounds (Pizzarello and Shock, 2010). As a comparison for the insoluble organic matter (IOM) within the carbonaceous chondrite samples, a kerogen type IV sample was also included. Kerogen is not a structural analogue to IOM, but type IV, and primitive chondrites share common organic contents (Matthewman et al. 2013), and kerogen represents recalicitrant macromolecular carbon. The Type IV kerogen sample used in this study is from the Cretaceous-age Wealdon Beds at Durdle Door, Dorset, UK (Matthewman et al., 2013). Previous pyrolysis-gas chromatography-mass spectrometry analysis of this sample shows it comprises numerous aromatic and phenolic compounds (Montgomery et al., 2016).

2.2 Sample charaterisation

Iceland sediments and synthetic crystals were characterised with VNIR reflectance spectroscopy, and either Raman spectroscopy or X-ray Diffraction (XRD) to determine their mineralogical composition. VNIR analysis was achieved using a Spectral Evolution RS-3500 spectrometer measuring from 350 to 2500 nm with an illuminated contact probe. Reflectance measurments were normalized to a Spectralon© white reflectance standard. Raman spectroscopy was conducted using a Horiba LabRAM HR and 633 nm laser with acquisition time and laser power variable depending on individual sample response. Identification of Raman peaks was performed using the RRUFF database (Downs 2006). Quantiative XRD analysis was also conducted for the Mudstone sample to further constrain the mineralogy of this more heterogeneous sedimentary substrate. Samples were first crushed to <5 µm using an agate ball mill in acetone, then dried at 38 °C overnight. This was then back-packed into standard Philips sample holders to produce maximum random orientation. Prepared samples were analysed with a Philips PW1050 / Hiltonbrooks DG2 instrument. Mineral identification was done using DiffracPlus, using ICDD PDF4, and semi-quantification achieved using the Reitveld method in SiroQuant ver3., with sample quantification error ~10 %.

2.3 UV photoluminescence spectroscopy

Low temperature UV PL measurements of the sedimentary Iceland substrates were performed using the Hyperspectral Luminescence and Optical Spectroscopy (HeLIOS, Cross et al, 2013) instrument at Aberystwyth University, UK. Samples were cooled to (20 K) using a closed loop Helium cryostat, at a base pressure (at room temperature) of ~10^{-4} mbar. Thorlabs mounted LEDs fitted with collimating lenses were used for excitation, providing ~50 mW at 280 nm and 500 mW at 365 nm. UV emission spectra were measured using a Horiba Jobin Yvon iHR320 fitted with an automated filter wheel for order sorting and a 395 nm long pass (Schott GG 395) filter to exclude the excitation light. The wavelength scale of the spectrometer was calibrated using a mercury emission lamp. Room

temperature UV photoluminescence analysis was performed for the carbonaceous chondrite chips and synthetic crystal samples, using UV excitation and emission measurement as described above, with a 395 nm longpass filter. Finally, Kerogen and Murchison samples were further analysed using a tunable light excitation source (max 10 mW), attached to the same Horiba Jobin Yvon iHR320 combined with a 395 nm long pass filter. UV PL emission spectra are presented as either relative emission intensity (native PL response) or as normalised maximum emission spectra to enable direct cross-comparison of spectral shape and features between samples.

3. Results

3.1 Sample characterisation

Iceland sample 'Gypsum' has Raman peaks present at 145, 180, 413, 493, 620, 670, 1008 and 1136 cm^{-1} (Figure 1A), consistent with gypsum reference spectra. Paleolacustrine 'Mudstone' has a single broad Raman peak at ~1550 cm^{-1} (Figure 1A) consistent with the amorphous carbon G band. Sample 'Oxide' has hematite Raman peaks at 225, 294, 410, 490, 485, and 488 cm^{-1} (Figure 1A). The Kerogen sample has weak and broad carbon D-band (1350 cm^{-1}) and G-band (1580 cm^{-1}) peaks.

VNIR reflectance spectrum (Figure 1B) for sample Gypsum shows a clear H_2O triplet at 1.9 µm and an S-O band at 2.4 µm, consistent with the Raman identification of gypsum. Sample Oxide shows Fe^{3+} charge transfer bands at 0.5 and 0.9 µm, consistent with the identification of haematite with Raman spectroscopy, and also OH, H_2O, and Fe-OH bands at 1.4, 1.9 and 2.3 µm respectively. These collectively demonstrate the presence of an additional hydrated, and likely nanophase, FeOOH component not detected with Raman spectroscopy. Finally, the Mudstone has a broad Fe^{2+} band at 1 µm and Al-OH band at 2.2 µm, and Q-XRD analysis shows the sample comprises plagioclase (19 %),

pyroxene (16 %), smectite clays (11 %), chlorite (6 %), and zeolite (5 %), in addition to a large amorphous component (43 %) comprising basaltic glass clasts and palagonite gel based on thin section petrographic analysis (data not shown).

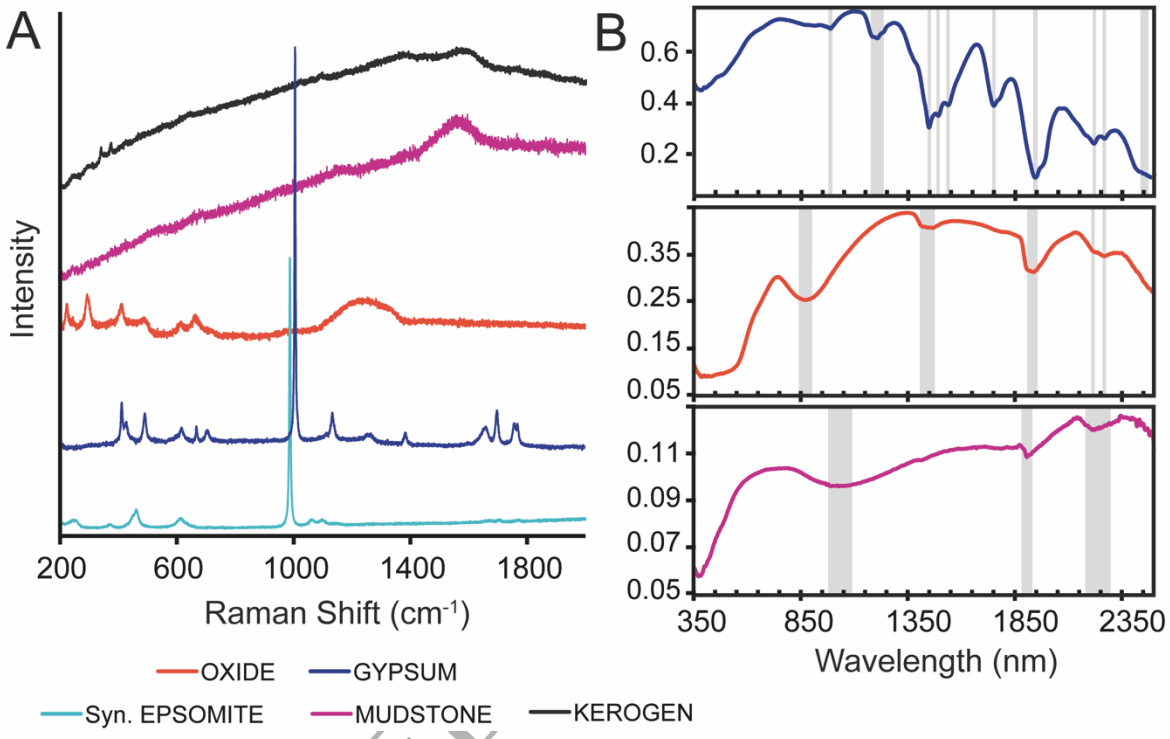

Figure 1. (A) Raman spectra (off-set for clarity) and (B) VNIR reflectance spectra (expressed as % reflectance) of Iceland sediment, synthetic epsomite, and Kerogen (Raman only). Absorption bands in (B) highlight spectral features discussed in the text.

3.2 UV PL of PAHs

Anthracene, perylene and pyrene show photoluminescence spectra that are markedly different to those of the Iceland sediment and kerogen samples (Figure 2). At 20 K, anthracene has 5 peaks, at 404, 420, 449 (λ_{ex} = 280 nm) or 459 (λ_{ex} = 365 nm), 470 (λ_{ex} = 280 nm) or 480 (λ_{ex} = 365 nm), and 513

nm. At 20 K perylene has 3 peaks at 532, 575 and 622 nm (λ_{ex} = 365 nm). Overall, the main emission response observed for anthracene is located at 400 - 500 nm, and 525 – 600 nm for perylene (Figure 2A). Pyrene also has an emission response between 400 – 500 nm, for both λ_{ex} = 280 nm and λ_{ex} = 365 nm (Figure 2B), with clear peaks observed with λ_{ex} = 365 nm at 440, 470, and 504 nm.

3.3 UV PL of sediment samples

The UV PL spectra of Mars analogue sediments are shown in Figure 2. Under 280 nm excitation (Figure 2C) a large, broad excitation response is observed between 400 – 600 nm for Mudstone, Kerogen, and Oxide samples, with the latter exhibiting an additional strong peak at 600 nm. The Gypsum sample exhibits a different response, with two well-defined peaks at 460 and ~570 nm. Under 365 nm excitation the resulting spectra reveal different responses in all samples, with Oxide, Mudstone and Kerogen samples showing three broad peaks between 450 and 650 nm, and a weaker peak observed at 715 nm. Kerogen has a further, well-defined emission peak at 408 nm that is absent in the sediment samples. Gypsum exhibits the same triplet of peaks between 450 and 650 nm as Oxide, Mudstone and Kerogen, with slight differences observed in their centre wavelengths. These peaks are more defined in the Gypsum sample, and sit on top of a larger, broad luminescence response centred at ~505 nm (Figure 2D).

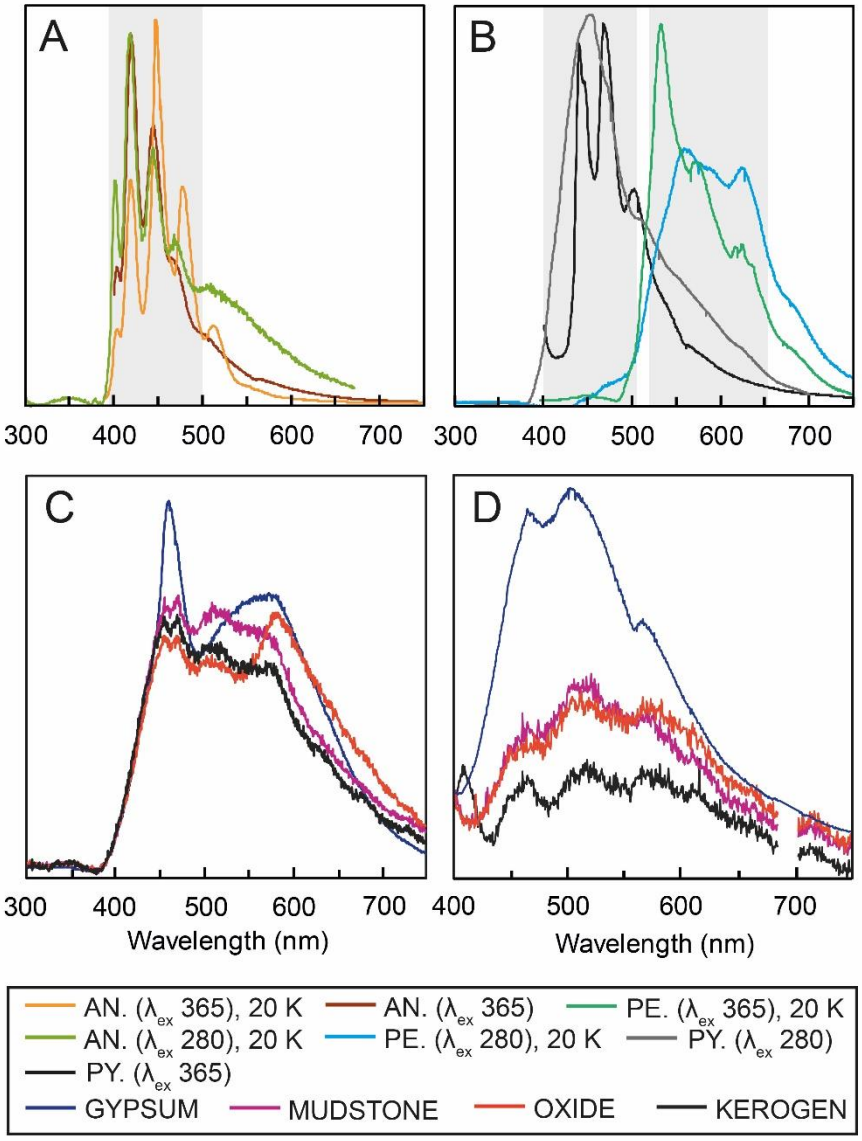

Figure 2. UV PL spectra of PAHs (A-B) measured at room temperature (except where stated at 20 K) and Iceland sediments measured at 20 K (C-D), with λ_{ex} = 280 and 365 nm. (A) Anthacene (AN.); (B) Perylene (PE.) and Pyrene (PY.); (C) Iceland sediment matrices and kerogen for λ_{ex} = 280 nm; and (D) Iceland sediment matrices and kerogen for λ_{ex} = 365 nm. All spectra normalised to maximum amplitude.

The UV PL spectra of the Iceland sediment matrices doped with each of the PAHs are shown in Figure 3. Differences in actual luminescence response are visible for Gypsum. Changes in the luminescence

spectra (λ_{ex} = 280 nm) here are seen in the addition of perylene and anthracene, both of which result in an increased luminescence at ~500 nm (Figure 3A), and a broadening of the whole luminescence peak. Under 365 nm excitation the addition of anthracene to gypsum causes a shift in centre wavelength in the resulting luminescence spectra from 505 nm to 530 nm (Figure 3D). Conversely, perylene does not produce such a response when doped onto gypsum, with no resulting shift towards the yellow where this PAH emits (Figure 3D). When doped with either of the PAHs, the Mudstone photoluminescence response shows only minimal changes with 280 nm excitation only, with the anthracene-doped Mudstone exhibiting an increased luminescence response at 580 nm (Figure 3B). The Mudstone doped with perylene, which while inconsistent with the perylene spectrum, produces a very similar luminescence response to the perylene-doped gypsum sample for 280 nm excitation. Finally, the presence of either PAH in the Oxide matrix has little to no effect on the resulting luminescence spectra, for either 280 nm or 365 nm excitation (Figure 3C and F).

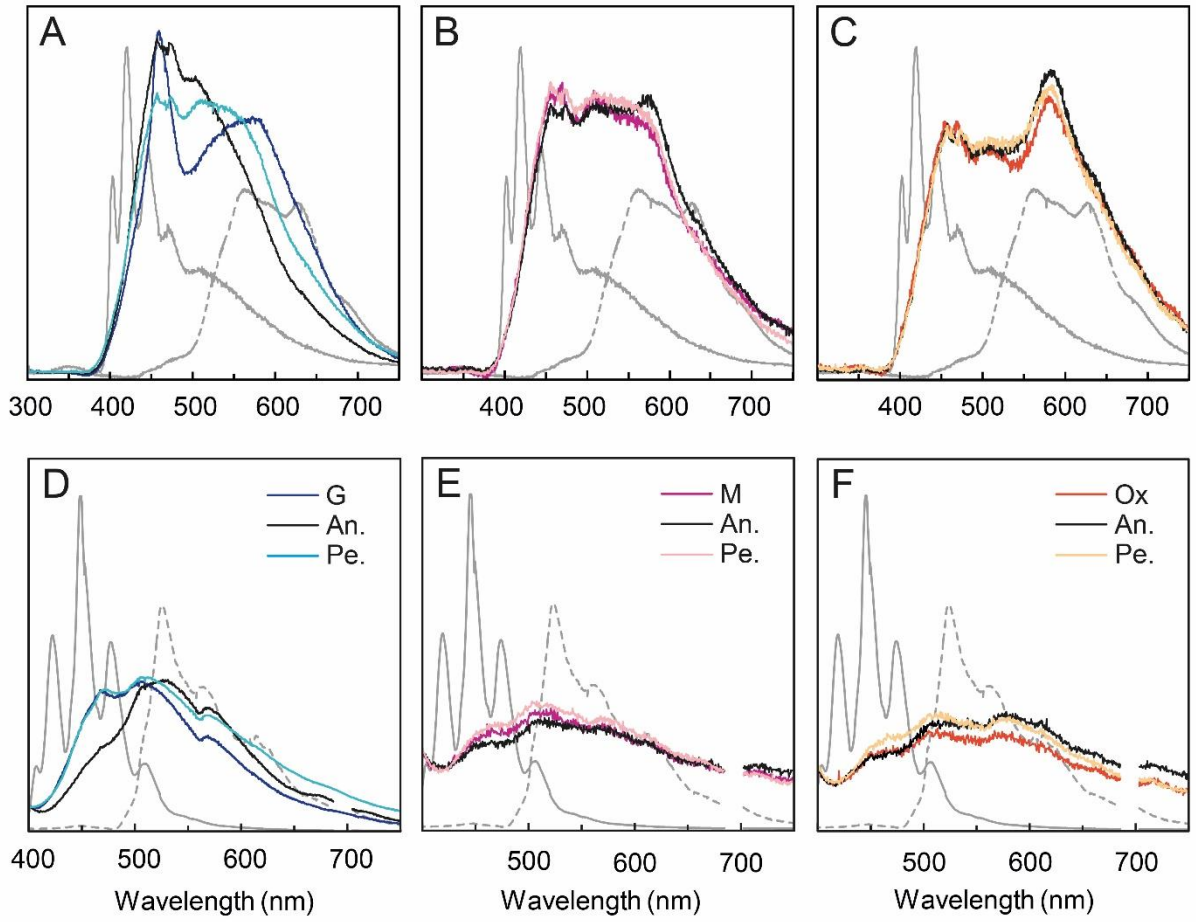

Figure 3. UV PL spectra of the pure Iceland sediment matrices and those doped with anthracene (An.) and perylene (Pe.) at λ_{ex} = 280 nm (A-C) and λ_{ex} = 365 nm (D-F) for Gypsum ('G', A+D), Mudstone ('M', B+E) and Oxide ('Ox', C+F). Pure PAH photoluminescence spectra are also shown in grey for comparison (solid line = anthracene, dashed line = perylene). All spectra normalised to maximum amplitude.

3.3 UV PL of synthetic salt crystals

The room-temperature UV PL spectra of the synthetic salt crystals, plus pyrene and anthracene, are shown in Figure 4. For the majority of samples, the addition of either PAH increases the luminescence response at λ_{ex} = 365 nm (Figure 4E-H). For halite under λ_{ex} = 365 nm, the addition of

anthracene produces a clear overprinting of the three largest anthacene peaks (at 412, 445 and 470 nm, Figure 4G) on the otherwise broad halite photoluminescence spectrum (Figure 4G), plus an additional, new peak at 580 nm. This effect is not seen under λ_{ex} = 280 nm (Figure 4C). For all the samples, under λ_{ex} = 365 nm the addition of iron oxide limits the photoluminescence response, with an additional red emission peak at 720 nm.

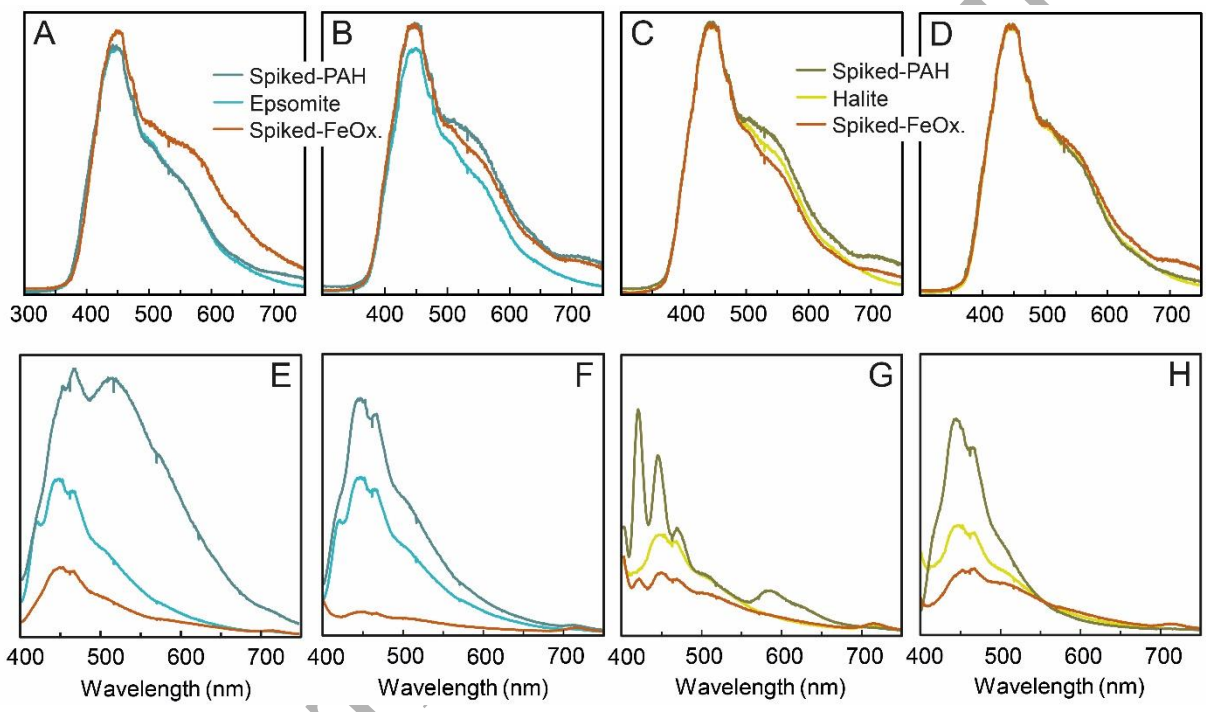

Figure 4. UV PL spectra of synthetic epsomite and halite at λ_{ex} = 280 nm (A -D) and λ_{ex} = 365 nm (E-H). Relative emission intensity data are shown for crystals doped with (i) anthracene (A, C, E, G) and pyrene (B, D, F, H), and (ii) anthracene or pyrene plus Fe oxyhydroxide ("Spiked-FeOx.").

3.4 UV luminescence of carbonaceous chondrites and Type IV Kerogen

The UV PL spectra for the carbonaceous chondrites are shown in Figure 5. All meteorites and the Type IV kerogen exhibit a strong blue luminescence response between 450 – 490 nm and an

additional red emission luminescence peak centred at ~720 nm (Figure 5A). This peak is strongest and most well-defined in the ALH84044, MET01072 and Type IV kerogen material. A broader peak centred around 515 – 520 nm is also seen in all meteorites and Type IV kerogen, which is strongest in Murchison "Face 2". The luminescence intensity differs between the different meteorites (Figure 5A), where Murchison produces the greatest luminescence response, followed by MET01072, ALH84044, and finally Kerogen, with the weakest luminescence response.

The evolution of UV PL response for Murchison "Face 2" and Type IV kerogen with increasing excitation wavelength from λ_{ex} = 225 to 375 is shown in Figure 5B. For both samples, the luminescence spectra become more resolved as excitation wavelength increases, whereby the overall emission narrows from a broad response between 400 – 600 nm at λ_{ex} = 225 nm to purely blue emission between 400 – 480 nm at λ_{ex} = 375 nm. Likewise, the number of resolvable peaks increases from 2 – 3 at the two shortest excitation wavelengths, to 5 resolvable peaks at the two longest excitation wavelengths. Finally, despite the presence of a 720 nm peak in the λ_{ex} = 365 nm luminescence spectra (Figure 5A), this peak is absent in the λ_{ex} = 225, 275, 325 and 375 nm luminescence spectra (Figure 5B).

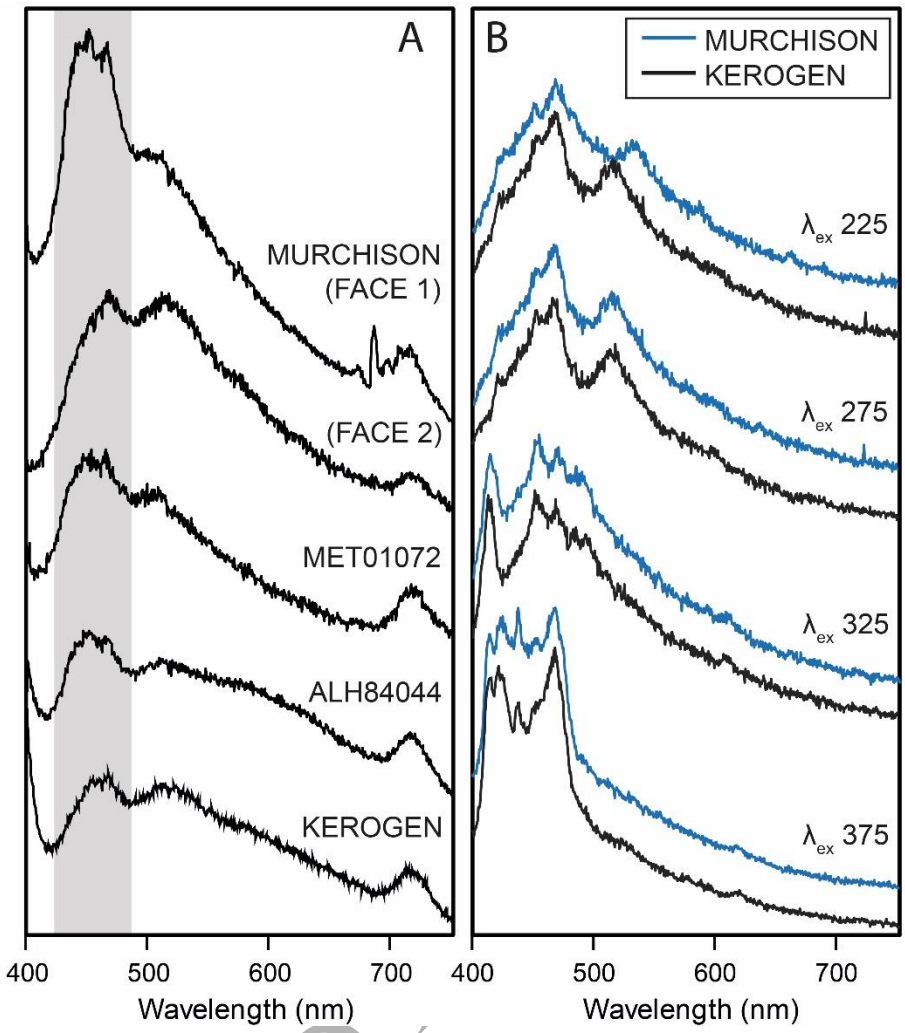

Figure 5. (A) Relative emission intensity UV PL spectra of carbonaceous chondrites and Type IV Kerogen, at λ_{ex} = 365 nm and room temperature. Two faces of Murchison are shown, one with a large visible chondrule ("Face 1") and one face without any visible chondrules ("Face 2"). The shaded band (430-480 nm) is the region of maximum photoluminescence; (B) UV PL spectra of Murchison (Face 2) and type IV Kerogen for λ_{ex} = 225, 275, 325, 375 nm at room temperature, with spectra normalised to maximum amplitude.

4. Discussion

4.1 Organic vs inorganic UV PL response

Across the entire sample set, only anthracene within the synthetic halite produces a photoluminescence signature that is visible within the broader, inorganic photoluminescence response (Figure 4G). In epsomite and pyrene-spiked halite, the addition of PAHs increases the resulting photoluminescence response, but not in a linear fashion as seen with the halite. This effect is also observed for the Gypsum sediment matrix, which produces a significantly different photoluminescence response when doped with either anthracene or perylene (Figure 3A and D). As such, it is possible that the detection of PAHs is related to the optical properties of the matrices, whereby the minerals that are most transparent to UV-visible wavelengths allow PAH excitation and detection of the resulting photoluminescence. This has relevance for target selection for UV PL interrogation during active surface missions, particularly given the prevalence of calcium sulfate diagenetic veins observed by the NASA Curiosity rover (Nachon et al., 2014; Rapin et al., 2016).

For the Mudstone and Oxide sediments, modification of the UV PL spectrum through the addition of PAHs is more subtle. The surface area measured beneath 8 wavelength regions covering the spectral response is shown in Figure 6. At λ_{ex} = 280 nm (figure 6-A-C), the presence of anthracene and perylene produce an increase (between 40 and 80%) in the 400 - 440 nm wavelength interval. This is consistent with the presence of the maximum wavelength emission for 2-5 ring PAHs being previously reported to be at 425 nm (Elsheman et al. 2018).

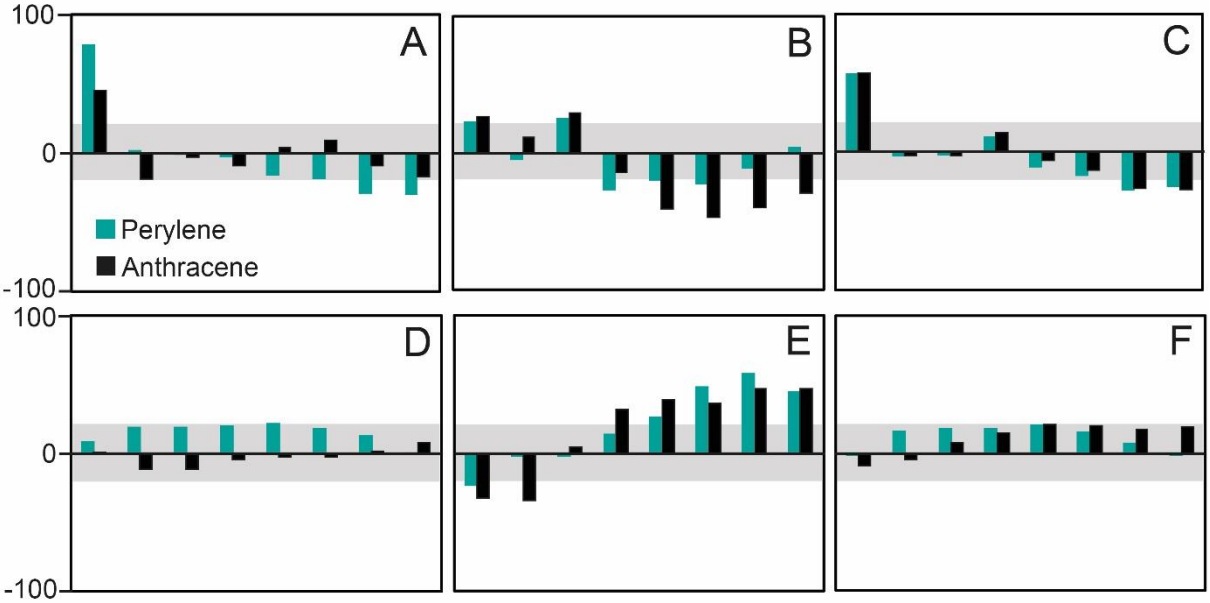

Figure 6. Surface area photoluminescence difference (%) across eight 40 nm spectral bins between 400 and 750 nm for sediment samples spiked with anthracene or perylene compared to their undoped matrices, at 280 nm (A-C) and 365 nm (D-F), for Mudstone (A and D), Gypsum (B and E) and Oxide (C and F). Grey region (+/- 20%) indicates differences due to inherent variation within the sample, defined by D and F.

All the carbonaceous chondrites and kerogen produce three photoluminescence ranges (450-465 nm, 500-520 nm, 700-720 nm), which are the combination of their organic and inorganic luminescent components, and as such unravelling their individual contributions is complex. Regarding inorganic contributions, the 450 nm peak could be ascribed to iron (Fe^{3+}, Zotov et al. 2002), as both chondrite chondrules and matrices are typically Fe^{3+} rich (Beck et al. 2012). In the case of Murchison "Face 1", the peak at 450 nm could be related to the presence of high iron content in the chondrule (where Fe/Mg ratios are typically below ~2; Hezel et al. 2018). The 465 nm peak observed can also be related to structural changes, such as the presence of lattice defects in forsterite (Karakus 1994), intrinsic defects in silica (Skuja et al. 1984a), and oxygen vacancies in silica (Tolmon et al. 1989), all of which

produce a strong photoluminescence response between 450 and 465 nm. A final possibility for the 450 nm luminescence peak would be a substitution of Al^{3+} for Si^{4+}, as observed in obsidian (Gaft et al. 2015), particularly as chondrite matrices are typically largely amorphous (Zolensky et al. 1993). In the green spectral region, the principal contribution at 510 nm and the absence of contribuation around 600-630 nm could result from the transition between the lowest energy levels of Mn^{2+} (Zotov et al. 2002), as Mn is detected even for concentration as low as 10 ppm (in the case of silicate glasses, Adrianasolo et al. 1989).

4.2 Photoluminescence of complex carbonaceous matter

The lowest photoluminescence response at λ_{ex} = 365 nm is observed for kerogen and the carbonaceous chondrites with the most complex carbon structures (ALH84044 and MET01072). This difference between the two Antarctic chondrites (ALH84044 and MET72072) and Murchison could result first from the extent of thermal alteration on the parent-body, where the least altered meteorites Murchison (2.5) and MET72072 (2.3) have a stronger luminescence response compared to ALH84044 (2). The gradual maturation induces an increase of the aromatic content and the decrease of volatiles such as H, O, N or S (Tissot and Welte, 1984), leading to lower photoluminescence response. For structures with a high number of rings, the energy gap between the ground and excited state become so low that it can overlap with vibrational transitions (Eshelman et al. 2017). The increase in aromatic ring concentration in the kerogen and CM2 meteorites investigated here results from a higher thermal maturity, and produces a reduced UV PL response (Hackley and Carrot 2016, and references therein). Apart from parent-body processes, the differences can also result from terrestrial weathering in Antarctica. Contrary to falls (e.g. Murchison), Antarctica finds may have suffered intense weathering, inducing the alteration of organics to an extent comparable to asteroidal conditions (Bland et al. 2006). As such, the thermal

maturity and alteration of organic carbon will have an influence on its *in-situ* detectability with UV photoluminescence on Mars, in addition to the effects imparted by the geological host substrate. **Shkolyar et al. (2018) performed time-gated UV luminescence analyses to measure the influence of martian substrate lithologies on kerogen detection, finding that kerogens are characterised by broad features between 400 and 500 nm, with a maximum emission around 430 nm, independent of the substrate. This is consistent with our results (Figure 5).**

Lastly, the surface environment of Mars is typified by high levels of radiation and a CO_2 rich atmosphere. This combined effect of ionising irradiation and an oxidising atmosphere can potentially modify complex organic matter and the associated photoluminescence responses. Previous experimental irradiation (442 nm laser, at a flux of 7 kW/m^2) of medium rank coals in an oxidising atmosphere have shown an increase in the UV photoluminescence emission after 3 hours (Eberhardt et al. 1992), and for all the samples the wavelength of maximum photoluminescence depended on the PAH ring number and carbon structure. Even considering the lower irradiance on Mars surface (0.59 kW/m^2, Visconti 2001), extended irradiation of complex organic on the surface of Mars may actually help their detection, by increasing their UV photoluminescence, counteracting the effect of thermal maturity. Regarding excitation, the kerogen sample in our study has a surface area of ~0.2 cm^2, which with an LED power of 500 mW results in a fluence of 2.5 W.cm^{-2}. This value is considerably lower than that provided by a pulsed laser (2.3 105 W.cm^{-2}, Shkolyar et al. 2018), suggesting pulsed laser excitation should be considered for future UV luminescence instruments.

4.3 Fe as a luminescence quencher

The addition of iron oxide has a significant effect on the UV PL signature. Under λ_{ex} = 365 nm, the addition of iron oxide limits the PL response, with an additional red emission peak at 720 nm (figure

4). The red region, and the 720 nm position are known to be related to the presence of Fe^{3+} (Zotov et al. 2002; Gaft et al. 2015). Alternatively, despite the presence of long-pass filter, the 720 nm could also potentially result from the second-order peak from 365 nm illumination itself. The lack of a 720 nm peak in the Kerogen and Murchison "Face 2" samples excited with the tunable light source (Figure 5B) is likely due to the relatively reduced power of the tunable source laser compared to the UV LEDs.

Iron oxide is known to be a UV photoluminescence quencher (Gaft et al. 2015). The presence of iron can increase the non-radiative transitions, resulting in the precipitation of the decay rate of the organic UV emitters, following a Stern-Volmer type quenching (Šima 2015 and references within). As a result, the radiation coming from the organic emitters would be absorbed by the iron oxide. Although this absorption is not complete, the presence of PAHs can be still be detected, particularly in salts (figure 4). Iron oxide affects Raman detection of organic material as well, where the addition of hematite on oxidised carbonaceous samples can impair carbon detection (Brolly et al. 2016). The presence of hematite can generate a broad band in the region of the carbon D-band (typically at 1350 cm^{-1}), possibly leading to misinterpretation regarding the presence of organic carbon. In that case, the combined use of Raman and UV PL can overcome both detection restrictions due to iron oxide, which is abundant on the surface of Mars.

Conclusions

UV photoluminescence analyses of Mars analogue sediments and synthetic salts doped with PAHs have been performed, for organic concentrations as low as 15 ppm (sediments) and 2 ppm (salts). Our results show that the resulting spectra deviate from both the undoped matrices and the pure PAHs spectra. Gypsum and halite show the most apparent spectral modifications when doped with

PAHs, and suggests that the most transparent minerals are more conducive to UV PL detection of trapped organic matter. Iron oxide, which is ubiquitously present on Mars, hampers but does not completely quench the UV PL signals produced by PAHs. Finally, the carbon maturity (resulting from secondary processes) influences the ability to detect carbonaceous matter, where thermal alteration and potential weathering may lower the UV PL response of meteoritic samples. Overall, UV photoluminescence is a promising but challenging technique, as the effects of substrate and iron oxides, and the nature of complex organic matter, are still largely unknown factors in determining detection limitations and capabilities within heterogeneous or natural materials. Our results are consistent with deep-UV (248.6 nm) observations, which reveal that native UV PL responses from inorganic mineral substrates do not occur below 360 nm, allowing effective discrimination between organic and inorganic targets (Beegle et al. 2015). We show that excitation at longer NUV wavelengths coupled with an analysis window that extends across the entire visible range can reveal combined spectral properties for both. This is observed particularly for complex organic matter within carbonaceous chondrites, with more spectral detail observed at longer excitation wavelengths. This forms a complementary approach should native UV PL prove a valuable technique for the *in situ* exploration of Mars, and therefore potentially elsewhere in the Solar System.

Acknowledgements

This project was supported by a Leverhulme Trust Research Project Grant (RPG-2015-071). C Cousins also wishes to acknowledge funding by the Royal Society of Edinburgh. The authors thank Geoff Bromiley for provision of the Type IV kerogen used in this study.

References

Abbey, W. J., Bhartia, R., Beegle, L. W., DeFlores, L., Paez, V., Sijapati, K., ... & Reid, R. (2017). Deep UV Raman spectroscopy for planetary exploration: the search for in situ organics. *Icarus*, *290*, 201-214.

Alexander, C. O. D., Bowden, R., Fogel, M. L., Howard, K. T., Herd, C. D. K., & Nittler, L. R. (2012). The provenances of asteroids, and their contributions to the volatile inventories of the terrestrial planets. *Science*, *337*(6095), 721-723.

Andrianasolo, B., Champagnon, B. & Duval, E. (1989). Behaviour of Mn^{2+} at very low concentrations in an aluminosilicate glass. Luminescence properties and electron paramagnetic resonance. *Physics and Chemistry of Glasses*, 30, 215-219.

Arvidson, R. E., Squyres, S. W., Anderson, R. C., Bell, J. F., Blaney, D., Brueckner, J., ... & Clark, B. C. (2006). Overview of the spirit Mars exploration rover mission to Gusev Crater: Landing site to Backstay Rock in the Columbia Hills. *Journal of Geophysical Research: Planets*, *111*(E2).

Ball, D. (2002). physical chemistry. *Cengage Learning publishing*.

Beck, P., De Andrade, V., Orthous-Daunay, F. R., Veronesi, G., Cotte, M., Quirico, E., & Schmitt, B. (2012). The redox state of iron in the matrix of CI, CM and metamorphosed CM chondrites by XANES spectroscopy. *Geochimica et Cosmochimica Acta*, *99*, 305-316.

Becker, L., Glavin, D. P., & Bada, J. L. (1997). Polycyclic aromatic hydrocarbons (PAHs) in Antarctic Martian meteorites, carbonaceous chondrites, and polar ice. *Geochimica et Cosmochimica Acta*, *61*(2), 475-481.

Beegle, L., Bhartia, R., White, M., DeFlores, L., Abbey, W., Wu, Y. H., ... & Edgett, K. S. (2015, March). SHERLOC: Scanning habitable environments with Raman & luminescence for organics & chemicals. In *Aerospace Conference, 2015 IEEE* (pp. 1-11). IEEE.

Bell, J. F., McSween, H. Y., Crisp, J. A., Morris, R. V., Murchie, S. L., Bridges, N. T., ... & Ghosh, A. (2000). Mineralogic and compositional properties of Martian soil and dust: Results from Mars Pathfinder. *Journal of Geophysical Research: Planets*, *105*(E1), 1721-1755.

Bland, P. A., Zolensky, M. E., Benedix, G. K., & Sephton, M. A. (2006). Weathering of chondritic meteorites. *Meteorites and the early solar system II*, 853-867.

Carrier, B. L., Beegle, L. W., Bhartia, R., & Abbey, W. J. (2016, March). Measurement of uv fluorescence and raman signatures of organic compounds in the subsurface of mars relevant minerals to constrain detection depth for the sherloc mars 2020 instrument. In *Lunar and Planetary Science Conference* (Vol. 47, p. 2660).

Chen, W., Westerhoff, P., Leenheer, J. A., & Booksh, K. (2003). Fluorescence excitation− emission matrix regional integration to quantify spectra for dissolved organic matter. *Environmental science & technology*, *37*(24), 5701-5710.

Cross, R.E., Gunn, M., Jones, G.O., Langstaff, D.P. and Evans, D.E. (2013). Hyperspectral optical imaging for material characterisation. *UK Luminescence and ESR Meeting*.

Dartnell, L. R., Desorgher, L., Ward, J. M., & Coates, A. J. (2007). Modelling the surface and subsurface martian radiation environment: implications for astrobiology. *Geophysical research letters*, *34*(2).

Dartnell, L. R., Storrie-Lombardi, M. C., Mullineaux, C. W., Ruban, A. V., Wright, G., Griffiths, A. D., ... & Ward, J. M. (2011). Degradation of cyanobacterial biosignatures by ionizing radiation. *Astrobiology*, *11*(10), 997-1016.

Dartnell, L. R., Patel, M. R., Storrie-Lombardi, M. C., Ward, J. M., & Muller, J. P. (2012). Experimental determination of photostability and fluorescence-based detection of PAHs on the Martian surface. *Meteoritics & Planetary Science*, 47(5), 806-819.

Derenne, S., & Robert, F. (2010). Model of molecular structure of the insoluble organic matter isolated from Murchison meteorite. *Meteoritics & Planetary Science*, *45*(9), 1461-1475.

Downs, R.T., 2006. The RRUFF Project: an integrated study of the chemistry, crystallography, Raman and infrared spectroscopy of minerals. program and abstracts of the 19th general meeting of the international mineralogical association in Kobe, 03–13.

Eberhardt, J. E., Nguyen, T. H., & Read, R. (1992). Fluorescence alteration of coal and polycyclic aromatic hydrocarbons. *Organic geochemistry*, *18*(2), 145-153.

Edgett, K. S., Yingst, R. A., Ravine, M. A., Caplinger, M. A., Maki, J. N., Ghaemi, F. T., ... & Heydari, E. (2012). Curiosity's Mars hand lens imager (MAHLI) investigation. *Space science reviews*, *170*(1-4), 259-317.

Ehlmann, B. L., Mustard, J. F., Fassett, C. I., Schon, S. C., Head III, J. W., Des Marais, D. J., ... & Murchie, S. L. (2008). Clay minerals in delta deposits and organic preservation potential on Mars. *Nature Geoscience*, *1*(6), 355.

Ehlmann, B. L., & Mustard, J. F. (2012). An in-situ record of major environmental transitions on early Mars at Northeast Syrtis Major. *Geophysical research letters*, *39*(11).

Eigenbrode, J. L., Summons, R. E., Steele, A., Freissinet, C., Millan, M., Navarro-González, R., ... & Archer, P. D. (2018). Organic matter preserved in 3-billion-year-old mudstones at Gale crater, Mars. *Science*, *360*(6393), 1096-1101.

Eshelman, E., Daly, M. G., Slater, G., Dietrich, P., & Gravel, J. F. (2014). An ultraviolet Raman wavelength for the in-situ analysis of organic compounds relevant to astrobiology. *Planetary and Space Science*, *93*, 65-70.

Eshelman, E., Wanger, G., Manatt, K., Malaska, M., Willis, M., Abbey, W., ... & Lane, A. L. (2017, December). WATSON: Detecting organic material in subsurface ice using deep-UV fluorescence and Raman spectroscopy. In *AGU Fall Meeting Abstracts*.

Eshelman, E., Daly, M. G., Slater, G., & Cloutis, E. (2015). Time-resolved detection of aromatic compounds on planetary surfaces by ultraviolet laser induced fluorescence and Raman spectroscopy. *Planetary and Space Science*, *119*, 200-207.

Eshelman, E., Daly, M. G., Slater, G., & Cloutis, E. (2017). Detecting aromatic compounds on planetary surfaces using ultraviolet time-resolved fluorescence spectroscopy. *Planetary and Space Science*.

Ehrenfreund, P., Röling, W. F. M., Thiel, C. S., Quinn, R., Sephton, M. A., Stoker, C., ... & Kidd, R. D. (2011). Astrobiology and habitability studies in preparation for future Mars missions: trends from investigating minerals, organics and biota. *International Journal of Astrobiology*, *10*(3), 239-253.

Fisk, M. R., Pommerenck, J., Watkins-Brandt, K., Edgett, K. S., Minitti, M. E., Hardgrove, C. J., ... & Kennedy, M. R. (2015, December). UV-Excited Fluorescence of Rocks in Gale Crater, Mars. In *AGU Fall Meeting Abstracts*.

Flynn, G. J., & McKay, D. S. (1990). An assessment of the meteoritic contribution to the Martian soil. *Journal of Geophysical Research: Solid Earth*, *95*(B9), 14497-14509.

Frantseva, K., Mueller, M., ten Kate, I. L., van der Tak, F. F., & Greenstreet, S. (2018). Delivery of organics to Mars through asteroid and comet impacts. *Icarus*, *309*, 125-133.

Freissinet, C., Glavin, D. P., Mahaffy, P. R., Miller, K. E., Eigenbrode, J. L., Summons, R. E., ... & Franz, H. B. (2015). Organic molecules in the sheepbed mudstone, gale crater, mars. *Journal of Geophysical Research: Planets*, *120*(3), 495-514.

Gaft, M., Reisfeld, R., & Panczer, G. (2015). *Modern luminescence spectroscopy of minerals and materials*. Springer.

Glavin, D. P., Freissinet, C., Miller, K. E., Eigenbrode, J. L., Brunner, A. E., Buch, A., ... & Cabane, M. (2013). Evidence for perchlorates and the origin of chlorinated hydrocarbons detected by SAM at the Rocknest aeolian deposit in Gale Crater. *Journal of Geophysical Research: Planets*, *118*(10), 1955-1973.

Golden, D. C., Ming, D. W., Morris, R. V., & Graff, T. G. (2008). Hydrothermal synthesis of hematite spherules and jarosite: Implications for diagenesis and hematite spherule formation in sulfate outcrops at Meridiani Planum, Mars. *American Mineralogist*, *93*(8-9), 1201-1214.

Fuchs, L. H., Olsen, E., & Jensen, K. J. (1973). Mineralogy, mineral-chemistry, and composition of the Murchison (C2) meteorite.

Goetz, W., Hecht, M. H., Hviid, S. F., Madsen, M. B., Pike, W. T., Staufer, U., ... & Edgett, K. S. (2012). Search for ultraviolet luminescence of soil particles at the Phoenix landing site, Mars. *Planetary and Space Science*, *70*(1), 134-147.

Golombek, M. P., & McSween, H. Y. (2014). Mars: Landing Site Geology, Mineralogy, and Geochemistry. In *Encyclopedia of the Solar System (Third Edition)* (pp. 397-420).

Grotzinger, J. P., Sumner, D. Y., Kah, L. C., Stack, K., Gupta, S., Edgar, L., ... & Milliken, R. (2014). A habitable fluvio-lacustrine environment at Yellowknife Bay, Gale Crater, Mars. *Science*, *343*(6169), 1242777.

Hackley, P. C., & Cardott, B. J. (2016). Application of organic petrography in North American shale petroleum systems: A review. *International Journal of Coal Geology*, *163*, 8-51.

Hezel, D. C., Wilden, J. S., Becker, D., Steinbach, S., Wombacher, F., & Harak, M. (2018). Fe isotope composition of bulk chondrules from Murchison (CM2): Constraints for parent body alteration,

nebula processes and chondrule-matrix complementarity. *Earth and Planetary Science Letters*, *490*, 31-39.

Klingelhöfer, G. R. D. S., Morris, R. V., Bernhardt, B., Schröder, C., Rodionov, D. S., De Souza, P. A., ... & Foh, J. (2004). Jarosite and hematite at Meridiani Planum from Opportunity's Mössbauer spectrometer. *Science*, *306*(5702), 1740-1745.

Kokaly, R. F., Clark, R. N., Swayze, G. A., Livo, K. E., Hoefen, T. M., Pearson, N. C., ... & Klein, A. J. (2017). *USGS spectral library version 7* (No. 1035). US Geological Survey.

Langevin, Y., Poulet, F., Bibring, J. P., & Gondet, B. (2005). Sulfates in the north polar region of Mars detected by OMEGA/Mars Express. *Science*, *307*(5715), 1584-1586.

Loizeau, D., Mangold, N., Poulet, F., Bibring, J. P., Gendrin, A., Ansan, V., ... & Neukum, G. (2007). Phyllosilicates in the Mawrth Vallis region of Mars. *Journal of Geophysical Research: Planets*, *112*(E8).

Lindgren, P., Hanna, R. D., Dobson, K. J., Tomkinson, T., & Lee, M. R. (2015). The paradox between low shock-stage and evidence for compaction in CM carbonaceous chondrites explained by multiple low-intensity impacts. *Geochimica et Cosmochimica Acta*, *148*, 159-178.

Mahaffy, P. R., Webster, C. R., Cabane, M., Conrad, P. G., Coll, P., Atreya, S. K., ... & Brinckerhoff, W. B. (2012). The sample analysis at Mars investigation and instrument suite. *Space Science Reviews*, *170*(1-4), 401-478.

Matthewman, R., Martins, Z., & Sephton, M. A. (2013). Type IV kerogens as analogues for organic macromolecular materials in aqueously altered carbonaceous chondrites. *Astrobiology*, *13*(4), 324-333.

Millan, M., Szopa, C., Buch, A., Coll, P., Glavin, D. P., Freissinet, C., ... & Teinturier, S. (2016). In situ analysis of martian regolith with the SAM experiment during the first mars year of the MSL mission: Identification of organic molecules by gas chromatography from laboratory measurements. *Planetary and Space Science*, *129*, 88-102.

Karakus, M. (1994). Cathodoluminescence Microscopy, A Technique Uniquely Suited to the Solution of Refractory Wear Problems. In *Proc. of the International Ceramics Conference (Austceram'94)* (pp. 925-940).

Minitti, M. E., & McCoy, T. J. (2012, March). Assessing the Longwave Ultraviolet Fluorescent Characteristics of Martian Meteorites. In *Lunar and Planetary Science Conference* (Vol. 43).

Muller, J. P., Griffiths, A. D., Dartnell, L. R., & Ward, J. (2011, October). Recent developments on WALI for planetary exploration of PAH organics and micro-organisms. In *EPSC-DPS Joint Meeting 2011* (p. 1726).

Nachon, M., Clegg, S. M., Mangold, N., Schröder, S., Kah, L. C., Dromart, G., ... & Le Mouélic, S. (2014). Calcium sulfate veins characterized by ChemCam/Curiosity at Gale crater, Mars. *Journal of Geophysical Research: Planets*, *119*(9), 1991-2016.

Osterloo, M. M., Anderson, F. S., Hamilton, V. E., & Hynek, B. M. (2010). Geologic context of proposed chloride-bearing materials on Mars. *Journal of Geophysical Research: Planets*, *115*(E10).

Palme, H., Hezel, D. C., & Ebel, D. S. (2015). The origin of chondrules: Constraints from matrix composition and matrix-chondrule complementarity. *Earth and Planetary Science Letters*, *411*, 11-19.

Pizzarello, S., & Shock, E. (2010). The organic composition of carbonaceous meteorites: the evolutionary story ahead of biochemistry. *Cold Spring Harbor perspectives in biology*, *2*(3), a002105.

Rapin, W., Meslin, P. Y., Maurice, S., Vaniman, D., Nachon, M., Mangold, N., ... & Martínez, G. M. (2016). Hydration state of calcium sulfates in Gale crater, Mars: Identification of bassanite veins. Earth and Planetary Science Letters, 452, 197-205.

Richardson, J. H., & Ando, M. E. (1977). Sub-part-per-trillion detection of polycyclic aromatic hydrocarbons by laser induced molecular fluorescence. Analytical chemistry, 49(7), 955-959.

Rivera-Figueroa, A. M., Ramazan, K. A., & Finlayson-Pitts, B. J. (2004). Fluorescence, absorption, and excitation spectra of polycyclic aromatic hydrocarbons as a tool for quantitative analysis. Journal of chemical education, 81(2), 242.

Shkolyar, S., Eshelman, E. J., Farmer, J. D., Hamilton, D., Daly, M. G., & Youngbull, C. (2018). Detecting Kerogen as a Biosignature Using Colocated UV Time-Gated Raman and Fluorescence Spectroscopy. Astrobiology, 18(4), 431-453.

Šima, J. (2015). (Non) luminescent properties of iron compounds. Acta Chimica Slovaca, 8(2), 126-132.

Skuja, L. N., Streletsky, A. N., & Pakovich, A. B. (1984). A new intrinsic defect in amorphous SiO2: twofold coordinated silicon. Solid state communications, 50(12), 1069-1072.

Skulinova, M., Lefebvre, C., Sobron, P., Eshelman, E., Daly, M., Gravel, J. F., ... & Koujelev, A. (2014). Time-resolved stand-off UV-Raman spectroscopy for planetary exploration. Planetary and Space Science, 92, 88-100.

Storrie-Lombardi, M. C., Muller, J. P., Fisk, M. R., Griffiths, A. D., & Coates, A. J. (2008). Potential for non-destructive astrochemistry using the ExoMars PanCam. Geophysical Research Letters, 35(12).

Storrie-Lombardi, M. C., Muller, J. P., Fisk, M. R., Cousins, C., Sattler, B., Griffiths, A. D., & Coates, A. J. (2009). Laser-Induced Fluorescence Emission (LIFE): searching for Mars organics with a UV-enhanced PanCam. Astrobiology, 9(10), 953-964.

Ten Kate, I. L. (2010). Organics on Mars?. Astrobiology, 10(6), 589-603.

Tissot, B. P., & Welte, D. H. (1984). Diagenesis, catagenesis and metagenesis of organic matter. In *Petroleum Formation and Occurrence* (pp. 69-73). Springer Berlin Heidelberg.

Uckert, K., Grubisic, A., Li, X., Brinckerhoff, W. B., Cornish, T., Farcy, B., & Getty, S. A. (2018). IR resonance-enhanced organic detection with two-step laser desorption time-of-flight mass spectrometry. *Icarus*, *299*, 15-21.

Vago, J. L., Westall, F., Coates, A. J., Jaumann, R., Korablev, O., Ciarletti, V., ... & Rull, F. (2017). Habitability on early Mars and the search for biosignatures with the ExoMars Rover. *Astrobiology*, *17*(6-7), 471-510.

Vaniman, D. T., Bish, D. L., Chipera, S. J., Fialips, C. I., Carey, J. W., & Feldman, W. C. (2004). Magnesium sulphate salts and the history of water on Mars. *Nature*, *431*(7009), 663.

Visconti, G. (2001). Fundamentals of Physics and Chemistry of the Atmosphere. Berlin Heidelberg New York: Springer.

Wray, J. J., Milliken, R. E., Dundas, C. M., Swayze, G. A., Andrews-Hanna, J. C., Baldridge, A. M., ... & Clark, R. N. (2011). Columbus crater and other possible groundwater-fed paleolakes of Terra Sirenum, Mars. *Journal of Geophysical Research: Planets*, *116*(E1).

Webster, C. R., Mahaffy, P. R., Atreya, S. K., Flesch, G. J., Mischna, M. A., Meslin, P. Y., ... & Martín-Torres, J. (2015). Mars methane detection and variability at Gale crater. *Science*, *347*(6220), 415-417.

Webster, C. R., Mahaffy, P. R., Atreya, S. K., Moores, J. E., Flesch, G. J., Malespin, C., ... & Gomez-Elvira, J. (2018). Background levels of methane in Mars' atmosphere show strong seasonal variations. *Science*, *360*(6393), 1093-1096.

Zolensky, M., Barrett, R., & Browning, L. (1993). Mineralogy and composition of matrix and chondrule rims in carbonaceous chondrites. *Geochimica et Cosmochimica Acta*, *57*(13), 3123-3148.